Product Development of a New 2D Time-of-Flight Scan Laser

Mihaiela Iliescu*, Victor Vlădãreanu*[1], Mihai Serbanescu, Marian Lazar****

**Institute of Solid Mechanics, Romanian Academy,*
Constantin Mille, 15, Bucharest, Romania,
***R&D Department, SC Optoelectronica-2001 SA*
409 Atomistilor Str., Magurele, Ilfov, Romania
[1] Corresponding author

Abstract: The paper presents the most important stages of product development for a new 2D TOF laser range sensor suitable for an autonomous platform. Some essential Scan-Laser characteristics are real-time, high frequency, medium-distance, light weight, low price, low power consumption, and wide scan angle with good resolution (1cm), suitable for most applications. The basic technology for measuring the distance between the sensor and the objects is that of Time-of-Flight (TOF) of light waves and, thus, detection of the distance from time between transmitted and received waves. The collected data is further processed using neural networks and statistical inference. The specifications of the sensor prototype, the method for measuring distance and examples of experimental results are also evidenced.

Keywords: optical sensor, spinning mirror, laser radiation, distance, TOF scanner, linear regression, neural networks.

1. INTRODUCTION

High performance intelligent autonomous systems rely on real time 2D distance scanning sensors, as for example: autonomous robots, auto-platforms, automotive market for collision avoidance system and automatically guided vehicles. A range of sensors are available on the market developed for this purpose (www.mysick.com, 2014; www.ibeo-as.com 2014), but these widely used laser range sensors are too expensive, heavy and power inefficient for most consumers.

This paper presents some of the most important stages of development for a new product, the 2D TOF laser range sensor. The product has been designed, concept developed and prototype manufactured through the team work of specialists (including the authors) from an innovative SME, Optoelectronica-2001 SA and the Institute of Solid Mechanics, in Romania. It should be noted that, as with many successful products, the Scan-Laser is the result of joint efforts of scientific researchers and engineers from industry. This fact has been many times pointed out by specialists and decision makers (McKelvey, M., Olof Zaring, O., Ljungberg, D., 2015).

The new Scan-Laser product, is an obstacle detection sensor model, compact, lightweight, power-efficient and low cost (Serbănescu, M., Iliescu M., et. Al, 2014; www.optoel.ro, 2014)]. It has a real time scanning distance of 50 m for 5% black targets, 10 mm linear resolution, 180º scanning field with 0.72º angular resolution and 12.500 scanning points per second (50Hz scanning frequency), 4W power consumption and a production cost of less than 1.000 Euro.

The paper further presents the most important stages of product development that were implemented for the new product, Scan-Laser. These are congruent with the strategy outlined by Ulrich K.T. and Eppinger St. D. (2000), mentioned next.

0. Planning - the stage prior to approving the process development project, including presentation of development techniques and market objectives, etc.

1. Concept development - the stage dealing with identification of target market requirements.

2. System design - the stage when product architecture is defined and the subsystems and components are settled upon.

3. Detailed design - in this stage, complete specifications of components are defined and elements to be supplied are identified.

4. Testing and perfecting - the stage prototype manufacturing is performed.

5. Production - the „zero series" and further, when any necessary adjustments are done, the series, or mass production.

2. CONCEPT DEVELOPMENT AND SYSTEM DESIGN

This stage of new product development is based on identification of target market requirements and evaluation of the alternative product concepts.

Based on this, laser sensor parameters that need to be extended, when compared to the characteristics of existing similar products are: scanning distance, scanning frequency, angular resolution and measurement resolution.

Specifically, these parameters values were chosen to be:

- minimum 50 m scanning distance;

- minimum 50 Hz scanning frequency, real time data;
- maximum 1º angular resolution;
- maximum 1 cm distance resolution.

Obtaining a low price product involves intelligent use of common components from mass production, such as: laser diode, photoreceptor, cheap optics and common electronic components.

2.1 Initial parameter design

A minimum 50 Hz real time scanning frequency involves 20 ms time for one horizon scanning and data transmission, respectively, the scanning time for 180º is 10 ms.

A minimum of 1 degree angular resolution involves 360 scanning pulses. The time between two successive determinations is:

$$T_{1-scanning} = \frac{10,000}{180} = 55\,[\mu s] \qquad (1)$$

Within the time mentioned above, scanning at 50 m distance, the laser spot will be moved by 0,78 m, so for point measurement the effective measurement time must be limited at a maximum of 1/20 of $T_{1\text{-}Scanning}$. Thus 1 point in the field will be considered as 40mm wide.

As a result of the considerations mentioned above, the maximum expected time for one measurement is:

$$T_{scanning} = \frac{55}{20} = 2.75\,[\mu s] \qquad (2)$$

The light passed the twin 50 m distance in 333.5 ns, so the scanning time will be reduced by this value. Therefore, the solution is to use the Time-of Flight, TOF, or Phase difference techniques.

For the latter, the minimum modulation frequency is:

$$F_{\min} = \frac{100}{2.4165} = 41\,[\text{MHz}] \qquad (3)$$

This frequency is not suitable for low cost systems, so it is only practical to use the Time-of-Flight solution (Kostamovaara, J., Kurtti, S., Jansson J.P, 2012).

2.2 Overall design

Necessary laser power is given from the telemetric low (Shapiro, J., Capron, B and Harney, R, 1981):

$$\Pr = Pe \cdot \left(\frac{Ar \cdot Te \cdot Tr \cdot Kr}{4\pi \cdot d^2} \right) \cdot \exp(-2\tau d) \qquad (4)$$

where:

Pr represents the received power;

Pe – emission power;

Ar – receiving area;

Te – optical emission efficiency;

Tr – optical reception efficiency;

Kr – target reflection coefficient;

d – distance to target;

τ – atmospheric attenuation coefficient.

The limit conditions are as follows:

- Pr-min = Pe / 561478 for 50m scanning distance and usual black target (Kr = 0.1);
- Pr-max = Pe / 2175 for 0.3m scanning distance and usual white target (Kr = 0.9).

The simplest solution is to use a common SI photodiode, whose functionality limits are: maximum power dissipation and minimum discrimination power level.

In these conditions necessary power emission is 40W, so it is possible to use an OSRAM SPL-90_3 laser diode and a reception photodiode OSRAM SFH 203PFA (www.osram-os.com, 2014).

Recommendable optic geometry is to use collinear or quasi-collinear (parallel) emission and reception.

In fact, the mechanical solutions vary between a spinning 45º mirror with static receiver and emitter with spinning all. The cheaper and simplest solution is that of a spinning mirror with a collinear emission and reception. This co-linearity can usually be obtained with a 50% beam splitter or integrated emission into the receiver optic.

In both cases the telemetric low (4) for a specific environment condition, at the specific distance d, turns into:

$$\Pr = Pe \cdot \left(\frac{Ar \cdot K'}{As} \right) \qquad (5)$$

where:

Pr represents the received power;

Pe –emission power;

Ar –receiving area;

As – laser spot area at specific distance d;

K' –constant for one specific condition, distance and target reflection coefficient.

Due to the fact that the emission of laser diode is elliptical, with fast and slow axis and for a power efficient collimating system, the laser spot will be thin (1/200), so that equation (5) becomes:

$$\Pr = Pe \cdot \left(\frac{Ar \cdot K}{Ds} \right) \qquad (6)$$

where K dimension is of [mm^{-1}]

For a 50% beam splitter with integrated emission area, Ae, we get:

$$\Pr_A = \frac{Pe \cdot Ae \cdot K}{4 \cdot Ds} + \frac{Pe \cdot (Ar - Ae) \cdot K}{2 \cdot Ds} \qquad (7)$$

For an integrated emission area into the receptor area, equation (7) turns into:

$$\Pr_B = \frac{Pe \cdot (Ar - Ae) \cdot K}{Ds} \qquad (8)$$

The laser spot area at distance *d* is defined by the geometrical optic low:

$$Ds = \frac{Dd \cdot d}{fe} + De \qquad (9)$$

And

$$De = 2 \cdot fe \cdot tg(\theta / 2) \qquad (10)$$

where:

- Dd – is the emission diode laser area;

- d – working distance;

- fe – focal length of emission lens;

- De – diameter of emission lens;

-Dr – diameter of receiving lens;

- θ – maximum emission divergence angle.

For the values of:

- d = 50m - specifications

- Dd = 200µm for OSRAM SPL-90_3

- θ = 30º for OSRAM SPL-90_3

we get:

$$Ds = De + \frac{5360}{De} \text{ [mm]} \qquad (11)$$

For both mentioned cases we define the “gain of scanner”:

$$C = \frac{4 \cdot \Pr}{Pe \cdot K \cdot \pi} \qquad (12)$$

and the above equation turns into:

$$C_A = \frac{2 \cdot Dr^2 - De^2}{2 \cdot (De + \frac{5360}{De})} \qquad (13)$$

$$C_B = \frac{Dr^2 - De^2}{(De + \frac{5360}{De})} \qquad (14)$$

Using receiving optics with a diameter *Dr=50mm*, and solving the system of equations (13) and (14), it results the variation of the gain versus the laser emission diameter *De* – see Fig. 1.

The “gains” $\mathbf{C_A}$ and $\mathbf{C_B}$ don’t have a physical equivalent; they are only mathematical system-defined variables.

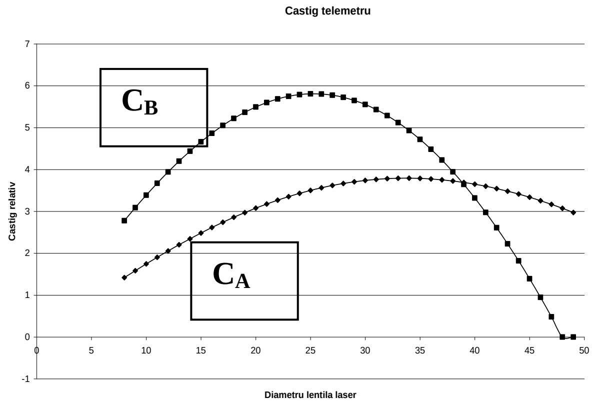

Fig. 1. Variation of C_A and C_B parameters versus *De*.

It can be noticed that there is a maximum of gains:

- C_A = 3.79 for De = 34mm - using a 50% beam splitter
- C_B = 5.80 for De = 25mm - for integrate emission in receiver optic.

Based on everything mentioned above, it is obvious that the optimal choice, under the initial circumstances, is to use the solution with *integrated emission in the receiver optics*, with a diameter of emission lens, De = 25mm.

2.3 Specific design

The chosen solution has a 45º spinning mirror at 3.000 rpm with concentric laser emission and receiver optics, and using Time-of-Flight technical solution for measuring distance.

Because TOF technique involves a well-known emission moment (www.osram-os.com, 2014), it is necessarily to have either a laser with integrated photodiode or an external photodiode across the laser beam.

The innovative adopted solution is to eliminate this necessity and measure directly the time between the laser command and the received signal from the target.

This solution adds an unknown dead time to the time measurement, but this time is dependent on the electronic components (gates, laser driver) and has a very slow time variation, a function of temperature and power supply value.

If at each rotation (or from time to time) this delay is measured by performing an internal self-shot (see Fig.2), this time error is eliminated. Moreover, the distance can now be measured not from the laser emission point but from the physical equipment – from the output laser window.

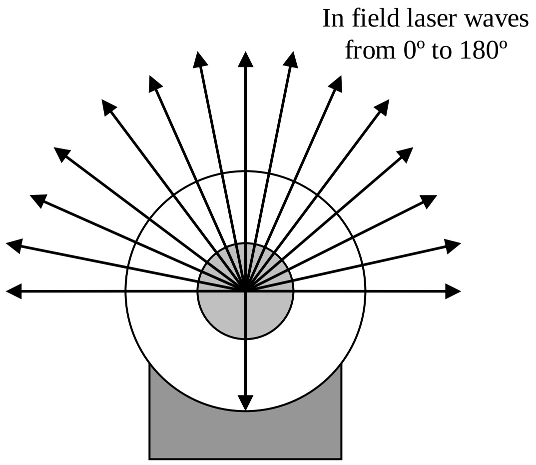

Fig.2 Scheme of the basic principle

The laser pulses have lengths of 40 ns…50 ns with a front of signal (rise time) of around 7 ns. The time between starting signal and receiving optical signal depends on the trigger point of reception and the amplitude of the received signal.

The laser signal rise time generates an error which has an upper limit of 1m – see Fig.3.

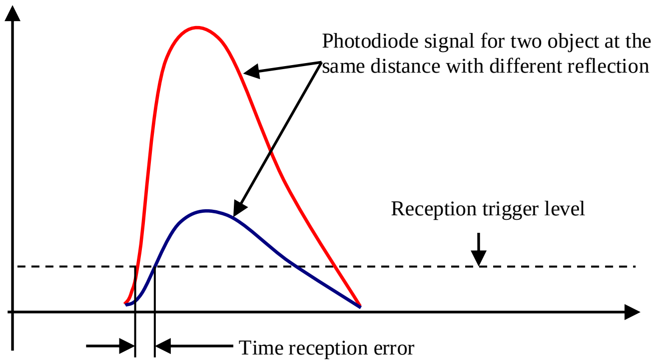

Fig.3 Photodiode received signals

This error can be eliminated, theoretically, by measuring the time between maximum waves points. Still, in field conditions, the received wave measurements are sometimes the sum of multiple reflection pulses and this technique cannot be applied.

The adopted solution is therefore to use multiple trigger points on the front of signal (rise time) and at the back (fall time) – see Fig. 4.

There are thus used 3 trigger points at fixed level to determine the time slope of signal – T0, T1 and T2 and T3, in order to finally determine the length of received signal.

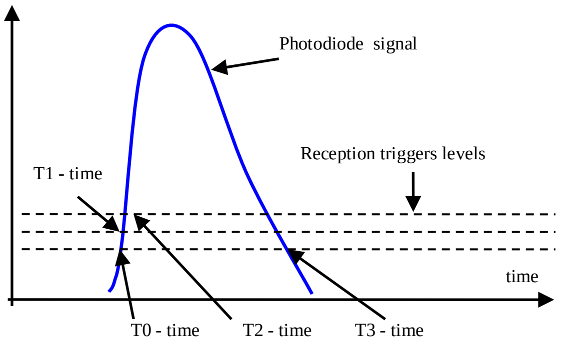

Fig.4 Received photodiode signal with triggers

In Fig 6 to Fig. 9, there are displayed the scanned points of an office room (see Fig.5) from T0-time, T1-time, T2-time and T3-time with expected distance determination error for small signal back reflection (in the corner, postcards on the wall etc.).

Fig.5 Office room used for experimental measurements

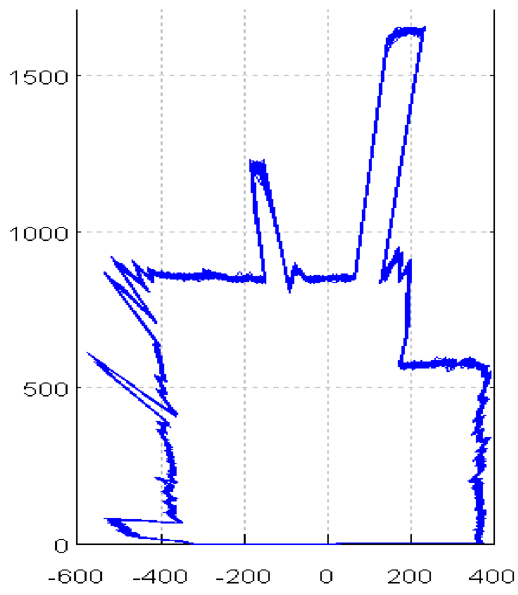

Fig.6 Distances generated from T0

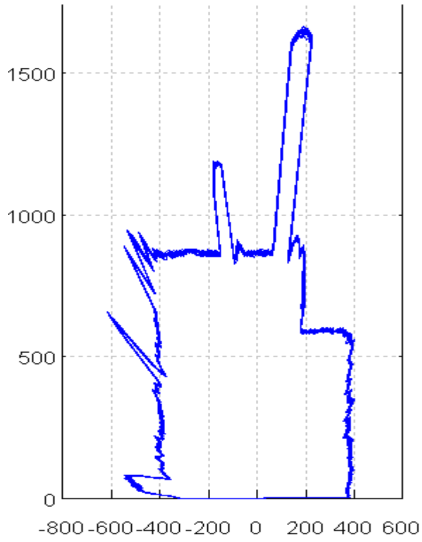

Fig.7 Distances generated from T1

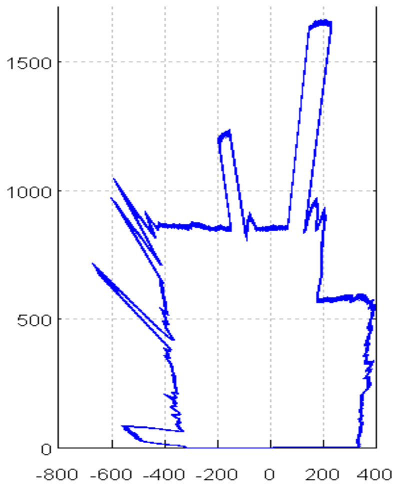

Fig.8 Distances generated from T2

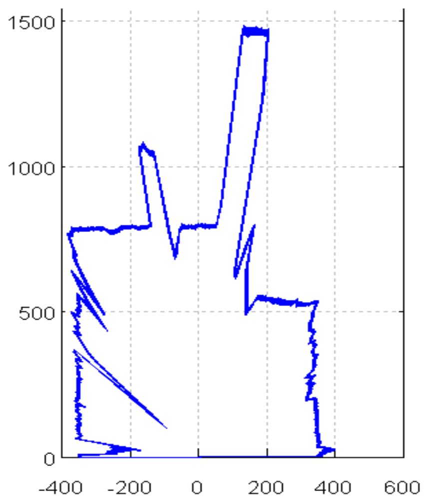

Fig.9 Distances generated from T3

The scale for all graphs is in [cm] and the figures show about 100 overlapped determinations. Line thickness defines the noise of the measurement.

There are two open doors that can be noticed in the figures, one from in office access area and one from a clipboard. In Fig.9 it can be seen where the back-reflection is low (and in the rest of the figures this generates slope error) the length of the signal is much small than the length of the starting laser signal (the objects are closer). From combinations of these measurements, the real distance and the real profile for the room will be determined – Fig.10.

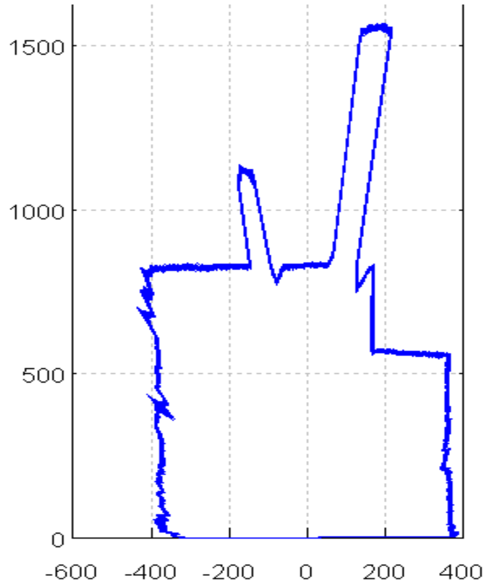

Fig.10 Determined room profile

In Fig.10 can be noticed the doors near the doors frame. On the left of the image the entire wall was full of postcards and scans reflect multiple variations of these reflections and in the middle left of the image (coordinate at -400 cm, 400 cm) there was a postcard with an unglued corner – see Fig.11.

Fig.11 Unglued postcard

Fig.12 shows the same office with its doors closed (100 measurements overlapped).

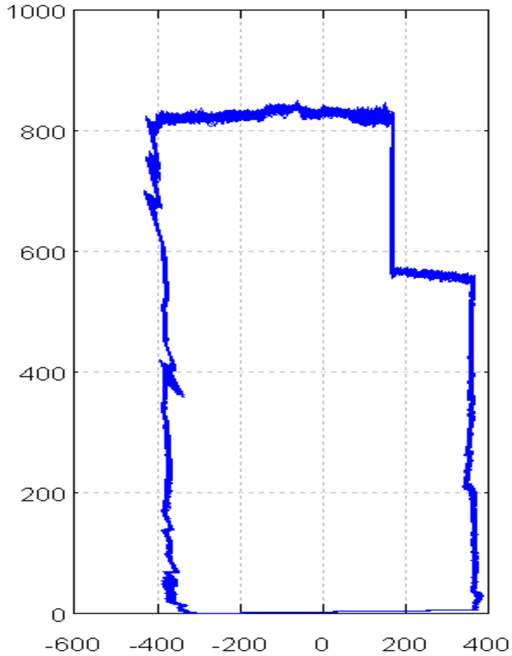

Fig.12 Determined room profile with doors closed

All the plotted data represents around 100 determinations overlapped used for data analyses and noise error estimations. The PC scanner software works in real time and the office room profile preview is displayed in Fig.13.

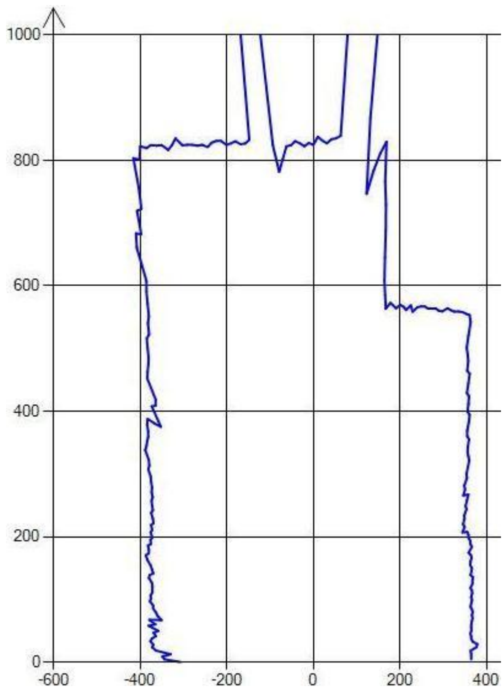

Fig.13 Real time determination

3. SENSOR DATA PROCESSING

The physical reality of the working environment makes processing the data received from the photodiode signal challenging. This is done using a number of trigger levels, as shown in Figure 4.

Under a certain threshold, signal measurement is indistinguishable from natural noise and is therefore unreliable. The first trigger is place slightly above this level and detects the beginning of a meaningful signal. The following two triggers determine the rising slope of the signal and are used in model verification. It is these three signals which will be used as input parameters for the estimation model.

The fourth trigger is on the back slope of an ideal isolated signal. This allows for computing the total time of a meaningful received signal, from which the distance to target is further inferred. While the theoretical approach seems to work, in practice several returning signals may interpolate into an unusable received signal. There is also the danger of higher amplitude noise being a factor in the sensor determination.

The measured distance was initially calculated as a function of the information obtained on the first (T0) and last (T3) triggers, using a mathematical relation. In order to no longer rely on the fourth trigger measurement, due to the reasons discussed above, it is required to estimate the value at the fourth trigger level (T3) from the values obtained from the previous three (T0 – T2). The resulting system will be integrated into the optical scanner software.

The raw data obtained from the sensor in continuous scanning mode is modelled using multivariate linear and non-linear regression and neural networks, using the mean values of each point at each of the four triggers. This was chosen from a number of possible approaches (Vladareanu, L., Sandru, O., 2009). The coding was done in Octave and Matlab.

Linear regression with multiple variables is used for the first regression model. The problem is of the form mentioned next:

$$Y = \hat{\theta} \cdot X \qquad (15)$$

$$X = [X_1 \quad X_2 \quad X_3] \qquad (16)$$

where:

X is a matrix containing the values of the three known triggers (T0-T2) for all 250 space points, plus an intercept term;

Y - vector containing all space point values for the fourth trigger (T3);

θ - matrix of parameters which estimate Y from X.

The issue revolves around finding the values of Θ which minimize the difference between the actual Y and the estimate obtained from the equation:

$$\hat{Y} = \theta_{LR} \cdot X \qquad (17)$$

The total sum of differences across all values is called the cost function (J). (Vladareanu, V., 2014)

The first step in a multiple variable regression model is to normalize the features and then run a batch gradient descent algorithm on the data, where each iteration minimizes the cost function by simultaneously updating all Θ parameters. Figure 14 shows a plot of the cost function J against the number of iterations (or epochs) of the gradient descent algorithm. As can be plainly seen the cost function decreases constantly to a convergence value.

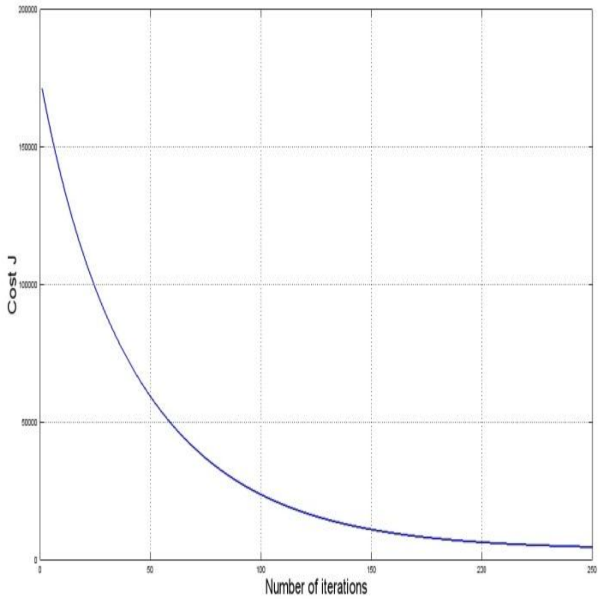

Fig.14 Linear Regression Cost Function

Gradient descent is an optimization algorithm where the potential solution is improved each iteration by moving along the feature gradient in the variable space. While it requires that the target function be differentiable and it is somewhat susceptible to local minima, gradient descent provides a stable and computationally inexpensive algorithm for function optimization.

There are a number of variants for gradient descent; the algorithm of choice here is batch gradient descent with a unity learning rate.

The same result can be achieved by using the closed-form solution to linear regression, called the normal equations of the problem. In vector form, this is:

$$\theta = \left(X^T \cdot X\right)^{-1} \cdot X^T \cdot \bar{y} \qquad (18)$$

which does not require any initial feature scaling.

In figure 15 there are plotted the values of the actual Y parameter against the fit obtained using linear regression with multiple variables with first-order features.

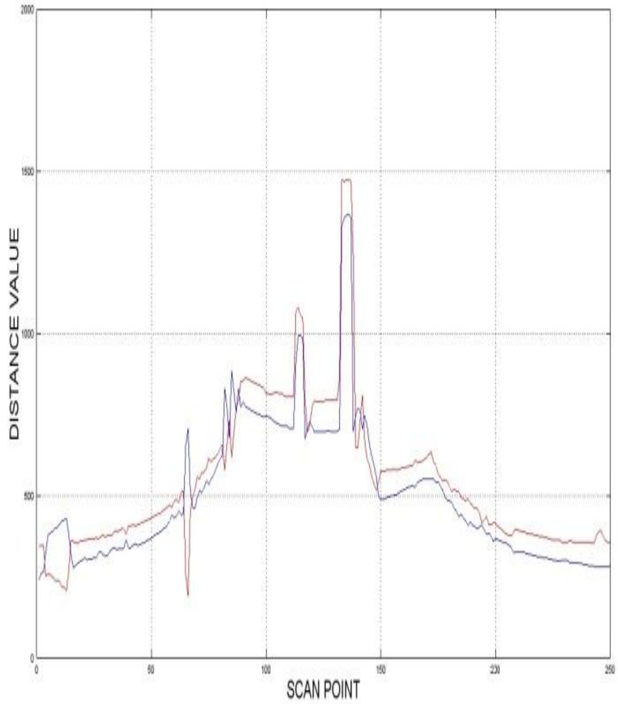

Fig.15 Real (red) and predicted (blue) values for single-order features

To obtain a better fit, a linear regression model using higher-order features is investigated.

The process is in essence the same with the important difference that we are trying to fit the data using a polynomial expression which includes all combinations of variables up to the sixth power.

The new hypothesis is described as follows:

$$Y = \hat{\theta} \cdot X \qquad (15)$$

$$X = [X_1 \quad X_2 \quad X_1X_2 \quad X_1^2 \quad \ldots \quad X_2^6] \qquad (19)$$

As it can be seen in Figure 16, the predicted values are closer to the known values measured empirically for Y.

Both versions of the linear regression model include regularization factors to prevent over-fitting. The regularization component is included in the cost function and provides a penalty for the data being fitted too closely using the polynomial variables.

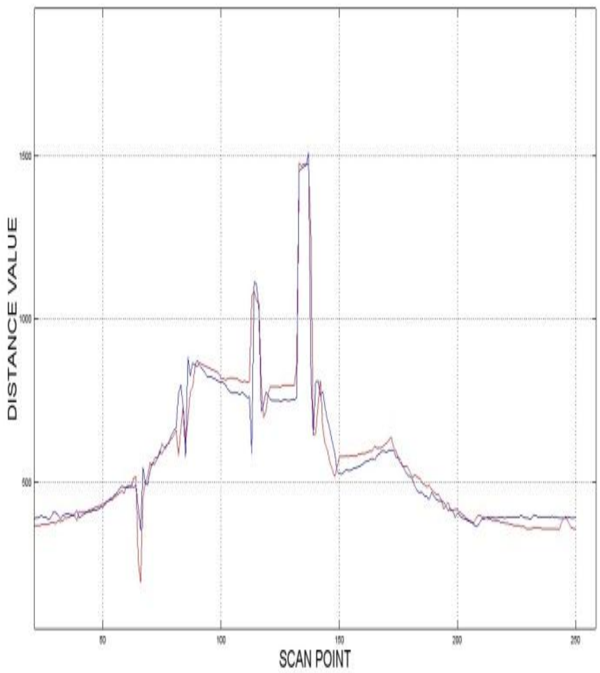

Fig.16 Real (red) and predicted (blue) values for multi-order features

The final model used is a feed-forward artificial neural network model.

An example of typical network topography is shown in Figure 17.

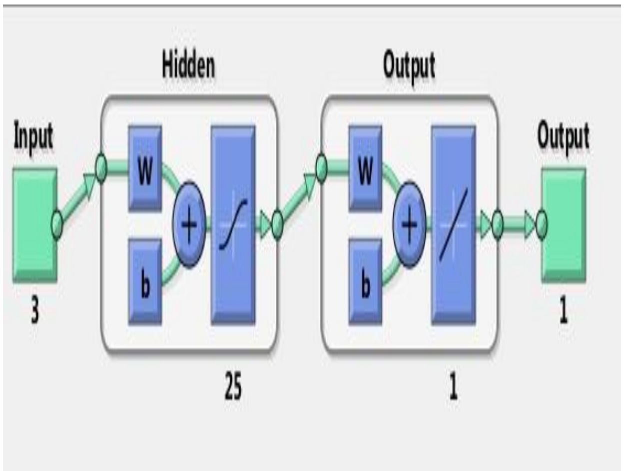

Fig.17 Artificial Neural Network with one hidden layer (25 neurons)

As is usually the case with training neural networks, approximately 70% of the available raw data is used for training, 20% for cross-validation after the initial training scenario, and 10% for testing.

Figure 18 shows the data fit using the best trained artificial neural network. After the network is trained, it can be used to generate new estimates given similar, but not necessarily identical, inputs to those previously encountered. As can be seen in this and in Figure 19, it provides the closest match of any of the three methods.

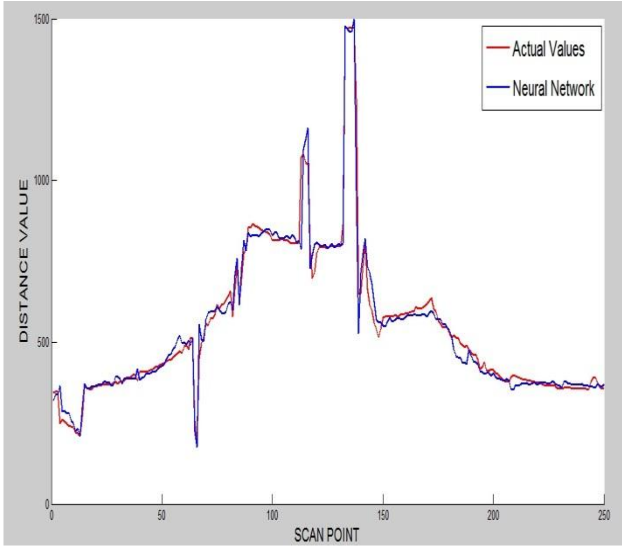

Fig.18 Comparison of real (red) and predicted values (blue) for a neural network

The results of the parameter estimation using linear regression with multiple variables and a trained artificial neural network can be seen in Figure 19.

As a result, the selected implementation is the artificial neural network with the trained weights, obtained through the simulation.

This will lead to faster and more robust results being obtained from the raw data, as well as the ability to run more tests using the prototype in actual situations (both static and dynamic) as part of a complex autonomous mechatronic platform – see refernce (Vladareanu, L., Tont, G., 2010).

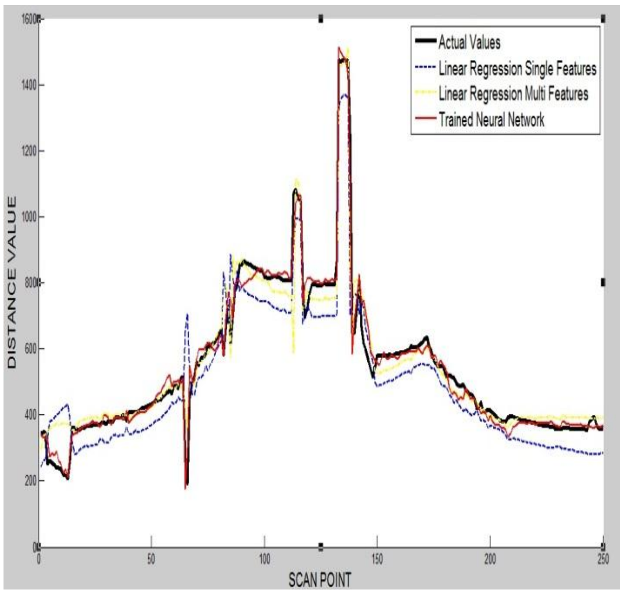

Fig.19 Comparison of real (black) and predicted values from all models

4. DETAIL DESIGN AND PRODUCT PROTOTYPE

Fig.20 presents the model for the configuration of the new product, Scan-Laser. Its main components are also outlined.

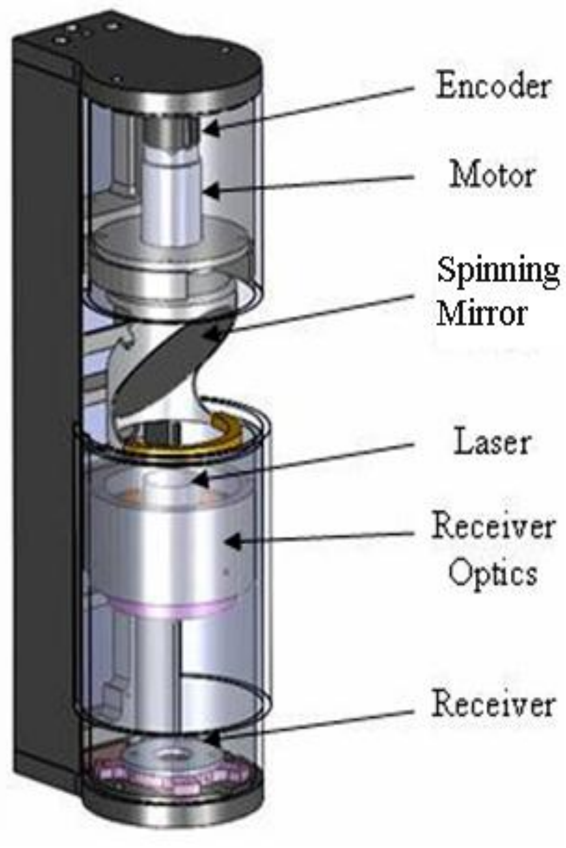

Fig.20 ScanLaser Prototype

The mechanical part of the scanner prototype was designed so as to ensure a perfect rotational axis for the spinning mirror subassembly, accurately aligned to hole system axis. More specifically, the moments of inertia on both OY and OZ axes had to be equal, so as to ensure mechanical equilibrium of the rotational system – see Figure 21.

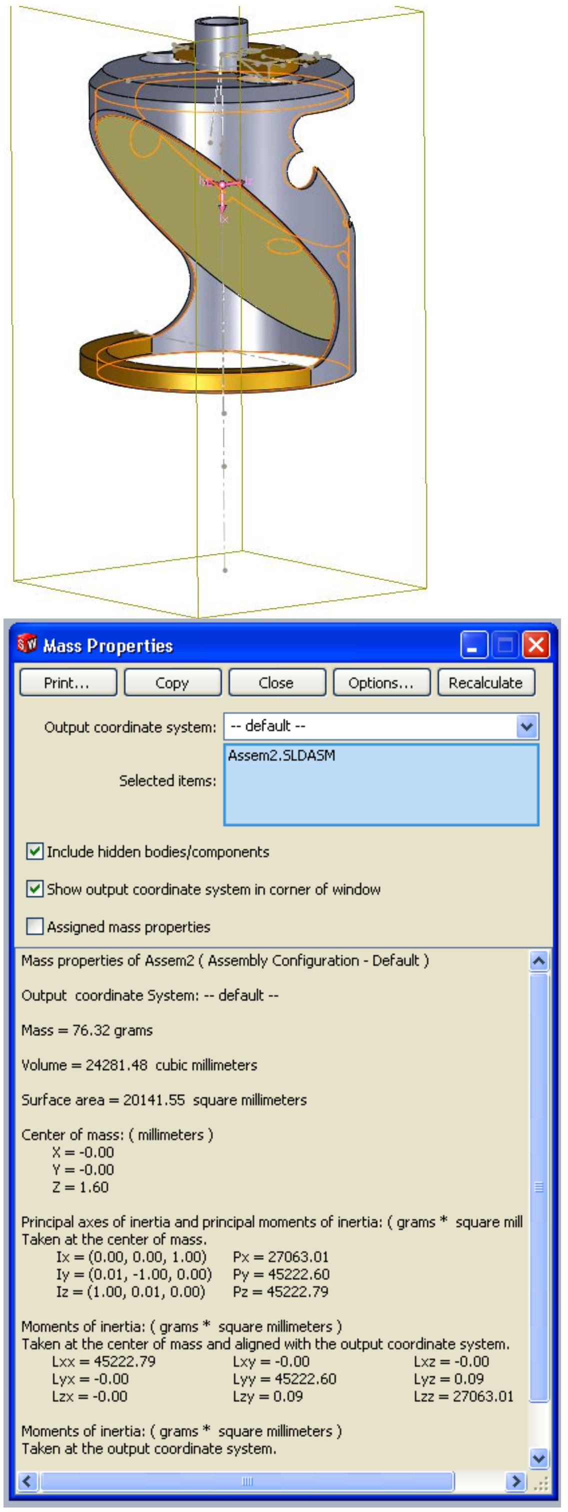

Fig. 21 Spinning mirror design

The materials of the spinning mirror subassembly components are as follows:

- Aluminium alloy – as low weight material for the main rotational component;

- Brass plates, made of AM63 – added as compensator weight for mechanical equilibrium when the spinning mirror rotates.

An image of the manufactured prototype subassembly is shown in Figure 22.

Fig. 22 Spinning mirror assembly manufactured prototype

For accurate manufacturing of Scan-Laser prototype's main component, the spinning mirror, both turning and milling techniques were used (Iliescu M., 2011).

Turning on a CNC lathe ensured the cylindrical profiles of the spinning component, including the one being coupled to driving motor's spindle. Further, CNC milling, on 5 axes vertical centre, ensured the precise generation of this component complex inner surfaces.

The brass plates, weight compensators, are accurately positioned by use of a video camera and then soldered to the required surfaces of main rotational component.

When all the system components are accurately fit together, dynamic calibration of the whole assembly is performed by rotating it at a 30 % higher value than the nominal rotational value in use.

Some other important TOF Scan-Laser components are presented next.

The motor encoder has 500 incremental positions with index output directly coupled with motor.

Correlated with the encoder output there was generated the laser pulse and the start of chronometer. The chronometer used is a MSC TDC-502 (www.msc-ge.com., 2014), a two channel 40 ps resolution counter.

The entire system is controlled from an ATMEL 8 bit microcontroller and external communications are made from the USB interface, serial interface with data communication speed 921.600 bauds or CAN bus.

The laser assembly has tilt adjustment, while the receiver has X-Y position adjustment for centring focused back-reflection with photodiode.

Thus, the schematic board of Scan-Laser is shown in Figure 23.

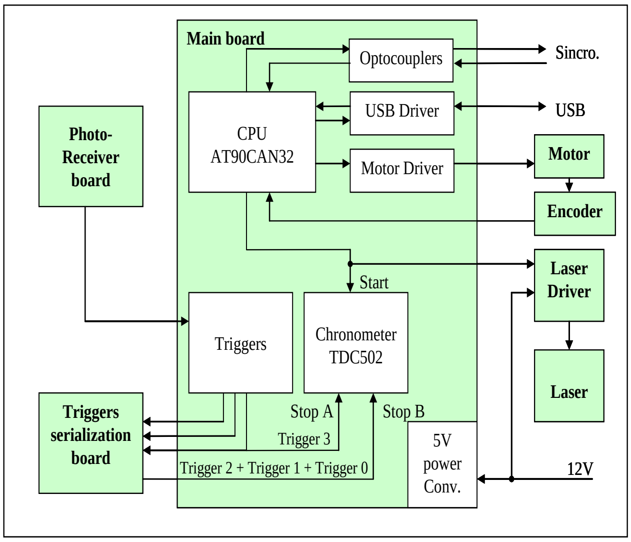

Fig.23 Schematic board of sensor

The MSC TDC-502 is a versatile time measurement integrated circuit, capable to measure time intervals between one common START impulse and multiple STOP impulses for two channels that work in parallel. The block diagram of MSC TDC-502 is detailed in Figure 24.

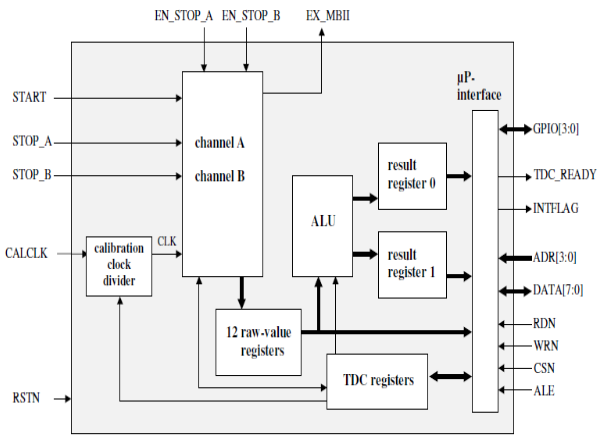

Fig.24 Schematic board of chronometer

The MSC TDC-502 can work in multiple time measurement configurations and for the specific scanner application the chosen working regime was with one START with two channels and four multiple STOPS each. The minimum time distance between two consecutive stops on one channel is 25ns. The working time diagram is displayed below (Figure 25):

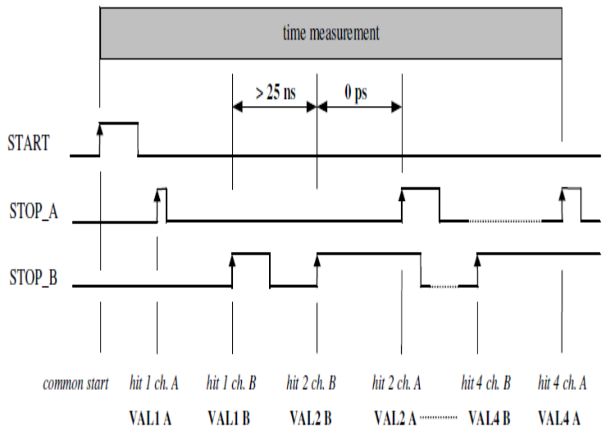

Fig.25 Time measurement for TDC-502 in specific mode

The three parallel triggers time with positive edge (T0,T1,T2) can be transformed in a serial signal with respects of T0,T1 and T2 times and a supplementary minimum 25ns between then – see Figure 26.

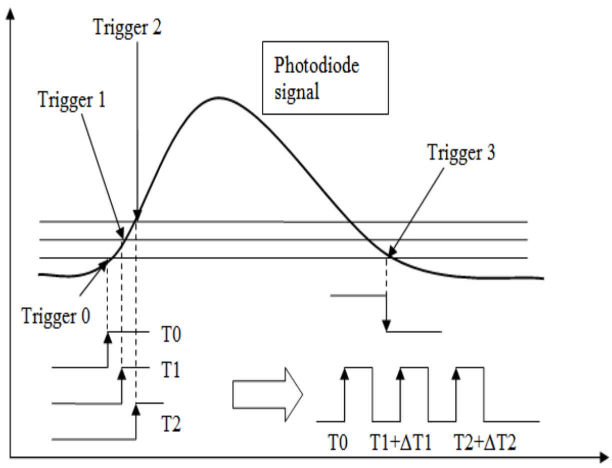

Fig.26 Serialization of triggers times

The resulting serial trigger will have supplementary delays ΔT1 and ΔT2 but at each rotation that the system makes a laser self-shot internally (see Fig.2), these time delays are measured and are subtracted from the measurements of intervals T0, T1 and T3.

The only limitations for ΔT1 and ΔT2 are that they must be larger than 25ns - from the TDC-502 constraint. In the channels within TDC-502 one is used for the positive edge of the serial signal for T0, T1 and T2 and one for the negative edge for the T3 trigger signal.

Figure 27 presents a field determination with buildings (top, right), vegetation (on left) and trees (middle).

There should be mentioned that the significance of a 0 value (as in plotted graph) is that there is no back-reflection from the field, meaning no information.

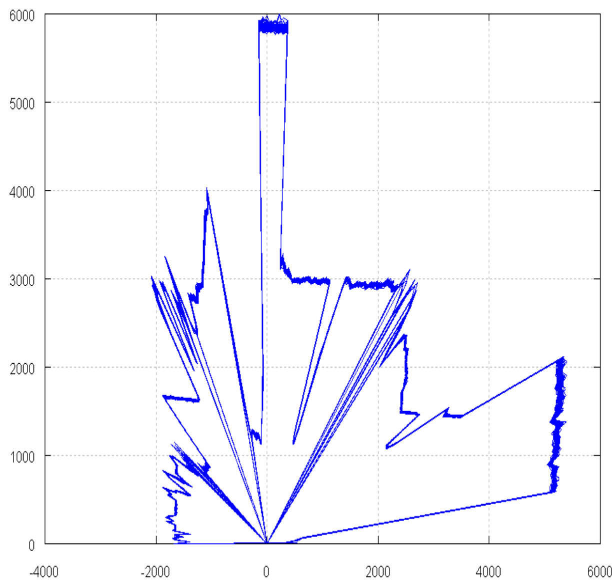

Fig.27 Plot of field determination

In summary, the overall performance of the new product Scan-Laser, measured and determined for the manufactured prototype, is shown next:

- scanning distance: 60m;
- scanning frequency: 50Hz (3000rpm);
- scanning angle 180º / 250 points;
- distance resolution: 1cm;
- angular resolution: 0.72º;
- power: 12V / 4W;
- weight: 850g;
- dimensions: 75 x 100 x 265mm;
- price: lower when compared to market offer of similar products, about 1.000 euro.

5. CONCLUSION

This paper presents some relevant aspects of the development and design of a 2D laser range sensor suitable for autonomous platforms.

The sensor features real-time, high frequency, medium-distance, lightweight, low price, low power consumption, and provides the wide scan angle with sufficient resolution (1cm), enough for most applications.

The raw results are processed using an artificial neural network obtained after thorough testing and comparison with other potential solutions. This allows an efficient software solution aimed at reducing measurement errors.

Further research involves the optimization of this sensor targeted on minimizing scan errors, dimensions and finally the transfer to the market, as well as integration into more complex autonomous systems for which several tests have been already run.

ACKNOWLEDGEMENT

This work was accomplished through the Partnerships Program in priority fields - PN II, developed with the support of MEN-UEFISCDI, PN-II-PT-PCCA-2013-4, ID2009, VIPRO project no.009/2014, Romanian Academy and FP7-PEOPLE-2012-IRSES RABOT project no. 318902

REFERENCES

Hybrid Pulsed Laser Diode 70 W Peak Power SPL LL90_3. & Silicon PIN Photodiode SFH203PFA & Range Finding Using Pulse Lasers Application Note OSRAM, www.osram-os.com, accessed on October, 2014

IBEO ScanLaser Products, http://www.ibeo-as.com

Iliescu, M., "Customized Products Manufacturing", Published by WSEAS Press, ISBN 978-960-474-303-2, 2011,

Kostamovaara, J. , Kurtti, S., Jansson, J.P. "A receiver – TDC chip set for accurate pulsed time-of-flight laser ranging", CDNLive! EMEA 2012, accessed at https://www.google.ro/webhp?sourceid=chrome-instant&ion=1&espv=2&ie=UTF-8#q=functionality+limist, on April, 20, 2015

McKelvey, M., Olof Zaring, O., Ljungberg, D., Creating innovative opportunities through research collaboration: An evolutionary framework and empirical illustration in engineering, Technovation39-40(2015)26–36,

http://www.optoel.ro/, accessed on November, 2015

Serbanescu, M., Iliescu, M., Lazar, M., Ciufudean, C., "Development of 2D, Ultra-Simple, Low-Cost, Optical Range TOF ScanLaser", Proceedings of the 5th International Conference on Circuits, Systems, Control, Signals (CSCS '14), pg. 91-96, ISSN: 1790-5117, ISBN: 978-960-474-374-2, Salerno, Italy, June, 2014.

Shapiro, J, Capron, B and Harney, R, Imaging And target detection with a heterodyne reception optical radar; Applied Optics, vol. 20 pp 3292 -3313, October 1981

SICK Products LMS5XX ScanLaser, https: //www.mysick.com, accessed on Octorber, 2014

TDC 502 user manual, www.msc-ge.com., accessed on September, 2014

Vladareanu, L., Sandru, O., Velea, L., Yu, H., The Actuators Control in Continuous Flux using the Winer Filters, Proceedings of Romanian Academy, Series A, vol.: 10 Issue: 1 Pg.: 81-90, 2009, ISSN 1454-9069

Vladareanu, L., Tont, G., Ion, I., Munteanu, M., S., Mitroi, D., "Walking Robots Dynamic Control Systems on an Uneven Terrain", Advances in Electrical and Computer Engineering, e-ISSN 1844-7600, vol. 10, no. 2, pp. 146-153, 2010,

Ulrich, K. ., Eppinger, S.D. Product Design and Development, MsGraw-Hill Companies, USA, 2000

Vladareanu, V., Contributions to intelligent control of autonomous robots equipped with multi-sensors systems, Ph.D. Thesis (summary), http://www.scribd.com/doc/274267670/Contributions-to-intelligent-control-of-autonomous-robots-equipped-with-multi-sensors-systems, Politehnica University Bucharest, 2014